EUROPEAN FUSION DEVELOPMENT AGREEMENT

EFDA–JET–PR(03)29

D. Moreau, F. Crisanti, X. Litaudon, D. Mazon, P. De Vries, R. Felton, E. Joffrin, L. Laborde, M. Lennholm, A. Murari, V. Pericoli-Ridolfini, M. Riva, T. Tala, G. Tresset, L. Zabeo, K.D. Zastrow and JET EFDA contributors

Real-Time Control of the Q-profile in JET for Steady State Advanced Tokamak Operation

Real-Time Control of the Q-profile in JET for Steady State Advanced Tokamak Operation

D. Moreau[1, 2], F. Crisanti[3], X. Litaudon[2], D. Mazon[2], P. De Vries[4], R. Felton[5], E. Joffrin[2], L. Laborde[2], M. Lennholm[2], A. Murari[6], V. Pericoli-Ridolfini[3], M. Riva[3], T. Tala[7], G. Tresset[2], L. Zabeo[2], K.D. Zastrow[5]
and JET EFDA contributors*

[1]EFDA-JET Close Support Unit, Culham Science Centre, Abingdon, OX14 3DB, U. K.
[2]Euratom-CEA Association, CEA-DSM-DRFC Cadarache, 13108, St Paul lez Durance, France
[3]Euratom-ENEA Association, C.R. Frascati, 00044 Frascati, Italy
[4]Euratom-FOM Association, TEC Cluster, 3430 BE Nieuwegein, The Netherlands
[5]Euratom-UKAEA Association, Culham Science Centre, Abingdon, U. K.
[6]Euratom-ENEA Association, Consorzio RFX, 4-35127 Padova, Italy
[7]Euratom-Tekes Association, VTT Processes, FIN-02044 VTT, Finland
**See annex of J. Pamela et al, "Overview of Recent JET Results and Future Perspectives", Fusion Energy 2000 (Proc. 18th Int. Conf. Sorrento, 2000), IAEA, Vienna (2001).*

Preprint of Paper to be submitted for publication in
Nuclear Fusion

Real-time control of the q-profile in JET for steady state advanced tokamak operation

D. Moreau[1, 2], F. Crisanti[3], X. Litaudon[2], D. Mazon[2], P. De Vries[4], R. Felton[5], E. Joffrin[2], L. Laborde[2], M. Lennholm[2], A. Murari[6], V. Pericoli-Ridolfini[3], M. Riva[3], T. Tala[7], G. Tresset[2], L. Zabeo[2], K.D. Zastrow[5] and contributors to the EFDA-JET workprogramme.

[1]EFDA-JET Close Support Unit, Culham Science Centre, Abingdon, OX14 3DB, U. K.
[2]Euratom-CEA Association, CEA-DSM-DRFC Cadarache, 13108, St Paul lez Durance, France
[3]Euratom-ENEA Association, C.R. Frascati, 00044 Frascati, Italy
[4]Euratom-FOM Association, TEC Cluster, 3430 BE Nieuwegein, The Netherlands
[5]Euratom-UKAEA Association, Culham Science Centre, Abingdon, U. K.
[6]Euratom-ENEA Association, Consorzio RFX, 4-35127 Padova, Italy
[7]Euratom-Tekes Association, VTT Processes, FIN-02044 VTT, Finland

Abstract

In order to simultaneously control the current and pressure profiles in high performance tokamak plasmas with internal transport barriers (ITB), a multi-variable model-based technique has been proposed. New algorithms using a truncated singular value decomposition (TSVD) of a linearised model operator and retaining the distributed nature of the system have been implemented in the JET control system. Their simplest versions have been applied to the control of the current density profile in reversed shear plasmas using three heating and current drive actuators (neutral beam injection, ion cyclotron resonant frequency heating and lower hybrid current drive). Successful control of the safety factor profile has been achieved in quasi steady state, on a time scale of the order of the current redistribution time. How the TSVD algorithm will be used in the forthcoming campaigns for the simultaneous control of the current profile and of the ITB temperature gradient is discussed in some detail, but this was not yet attempted in the present pioneering experiments.

1. Introduction

The control of so-called "advanced" plasma regimes [1-3] for steady state high performance tokamak operation is a challenge, in particular because of the non-linear coupling between the current density and the pressure profile, leading to the emergence and interplay between internal transport barriers (ITB), large bootstrap current fractions and plasma rotation, and weak or negative magnetic shear. In a burning plasma, the alpha-particle power will also be a strong function of these profiles, and, through its effect on the bootstrap current, will be at the origin of a large (though ultra-slow) redistribution of the current density. The possible destabilisation of adverse toroidal Alfvén eigenmodes (TAE) - such as the drift kinetic modes which are anticipated to appear at high values of the central safety factor [4] - as well as potential thermal instabilities due to the ITB dynamics will further complicate the issue.

A strategy for reaching a high performance plasma state in an advanced tokamak scenario is to preform an optimized current density profile early in the discharge by combining the skin effect (fast ohmic current ramp) with off-axis non-inductive currents. During this phase of the discharge, the low plasma density and pressure are beneficial for efficient current drive and for avoiding pressure driven instabilities at rational magnetic surfaces, respectively. A slow

interchange between the non-inductive current and the bootstrap component must then take place while the density rises together with intense plasma heating. Adequate plasma control will be required in order to maintain the pressure and current profiles close to their optimum shapes while approaching the steady state burn. Simulating the effect of feedback control loops for ITER has shown that, when the fusion amplification factor, Q, is large, the rise time of the bootstrap current is of paramount importance. Using a diagonal (uncoupled) 2-point control of the safety factor profile (q-profile), at the plasma center (q_0) and at mid-radius, it was then found that the characteristic ramp up time of the plasma density and, hence, fusion power and bootstrap current had to be at least as large as the full resistive current diffusion time, for q_0 to be controllable with reasonable amounts of external current drive power [5]. As far as experiments are concerned, real-time control of the internal inductance parameter - a measure of the current profile shape - has been achieved with LHCD on Tore Supra [6]. Improvement of plasma performance through active modification of the current density and pressure profiles in advanced plasma regimes with ITB's, through heating and current drive, or by inducing sheared plasma rotation, has also been the goal of intense research for example on TFTR [7], JT-60U [8-10], DIII-D [11], Alcator C-Mod [12] and JET [13-15]. Experimental investigations regarding the real-time (closed loop) control– of, *(i)* lumped parameters characterizing the pressure profile in ITB discharges [16], then *(ii)* of the full safety factor profile during the ITB preforming phase [17-18] and, more recently, *(iii)* of the full q-profile during the main heating phase of the discharges, have begun on JET. They will ultimately have to be carried out in burning plasmas, with high bootstrap current fractions, and over time scales which are much longer than the resistive diffusion time, in order to be fully reactor relevant.

This article addresses the methods which are being implemented on JET to control the pressure and current density profiles. Initial experimental results obtained with a combination of neutral beam injection (NBI), ion cyclotron resonant heating (ICRH) and lower hybrid current drive (LHCD) to control the q-profile are also presented. The proposed technique, which should be well adapted to control a distributed parameter system such as a set of coupled radial profiles, is described in the following section. It is based on a truncated singular value decomposition (TSVD) of a model integral operator (e.g. diffusion-like) in which the couplings between the pressure and current density profiles are intrinsically imbedded. How the general technique can be applied for the simultaneous control of these two profiles in advanced tokamak scenarios is discussed in some detail. In section 3, we describe a preliminary experiment using the simplest version of the algorithm where only one actuator (LHCD) was used. It will be shown that a satisfactory control of the q-profile can be achieved within the one-parameter family of profiles accessible with only one actuator, i.e. with a steady state offset between the requested profile and the achieved one which is minimum in the least square sense. In section 4, the first experiments using a multiple-input-multiple-output (MIMO) controller to control the q-profile with three heating and current drive actuators, namely NBI, ICRH and LHCD, will be reported. A conclusion will finally be given together with the prospects for future experiments aiming at the simultaneous control of the current and pressure profiles in steady state plasmas with ITB's.

2. A model-based SVD technique for real-time control of plasma parameter profiles

Early experiments on real-time control of ITB plasmas in JET [16] were based on a lumped parameter approach, i.e. on scalar measurements characterising the temperature profile, such as the maximum value across the plasma radius of the normalised temperature gradient, $\rho_T{*}_{max}$

(where ρ_T* is the local dimensionless ratio between the ion Larmor radius at the sound speed and the temperature gradient length [19]), and other global parameters such as the neutron rate, R_{NT}. But no attempt was made at estimating and controlling the current density profile in real time and, as a consequence, its slow evolution led to the loss of the ITB control after about 8 s, which is of the order of the current redistribution time. The coupled evolution of the pressure and current density profiles in ITB discharges occurs through complicated non-linear transport equations and the effect of feedback control loops on these profiles is not obvious in such regimes. Simulations have shown the limitations of controller designs based on decoupled loops, i. e. one-to-one correspondance between the available actuators (heating and current drive systems) and various global parameters or values of the safety factor at particular locations across the discharge (e. g. [5, 20]). More information on the spatial structure of the system can be taken into account by considering the distributed nature of the problem and the fact that various measured quantities at different radii are indeed related through a nonlinear, possibly diffusion-like, operator. Model-based control techniques have been applied to the design of MIMO controllers for nonlinear distributed parameter systems governing chemical processes [21]. It is tempting to apply such techniques to control the plasma profiles in tokamak discharges, in the aim of operating the device in the ITB regime and in steady state.

There is no general method to take into account non-linearities of models in the design of controllers, but to use linear response theory around an equilibrium which is assumed to be the target equilibrium that the controller should hold despite various disturbances. When such linearisation does not work, one can resort to specially adapted methods which are case-dependent and can sometimes improve the design, although without any generality (it may for instance happen that a system for which an analytical model exists becomes linear in some other variables than those which are to be controlled and in this case a change of variable can be appropriate). In the general case, the rationale underlying the use of linear response theory is indeed based on the observation that, if the controller is to provide stability around the required target, the system should never depart largely from the assumed equilibrium and therefore a control matrix which has been defined through linearisation can in many cases provide an acceptable solution to the problem. One can therefore anticipate that it may be important to develop open loop methods to bring the system close enough to the target before using the control algorithm to track the required setpoint and insure its stability. For triggering ITB's and operating tokamak plasmas in a high confinement advanced regime, such methods have been the subject of intensive research for the past few years. They are based on the application of high power heating during a current ramp which is believed to provide optimal ExB velocity shear and magnetic shear to stabilise microturbulence, and have now become reliable enough [7-15].

In the present experiments, we have therefore investigated the possibility of exerting linearised model-based feedback control in order to make further progress towards genuine steady state advanced tokamak operation. The methods which will be discussed below for this purpose can also, if necessary, be easily extrapolated to a more sophisticated technique known as model-based predictive control which is generally more powerful when nonlinearities are important, but at the expense of a larger computational power.

2.1 Truncated SVD, basis functions and model representation of a distributed parameter system

The first task one has to face before the proper design of a model-based controller can be started is to develop a suitable model to derive the approximate response functions of the

system. Without any loss of generality, the linearised response function of the current density and pressure output profiles (represented below by two functions of space and time, $y_1(x, t)$ and $y_2(x, t)$, respectively, where x stands for the normalised radius, t for time) to the various power input stimuli (e.g. LHCD, NBI and ICRH power deposition represented by functions $\pi_1(x, t)$, $\pi_2(x, t)$, $\pi_3(x, t)$, respectively) can be sought under the integral form :

$$\mathcal{Y}(x,t) = \int_0^t dt' \int_0^1 dx' \quad \mathcal{K}(x,x',t-t') \bullet \mathcal{P}(x',t') \qquad (1)$$

where $\mathcal{Y}(x, t)$ represents the vector $[y_1(x, t) , y_2(x, t)]$, $\mathcal{K}(x, x', \tau)$ is an unknown kernel and $\mathcal{P}(x, t)$ represents the source power deposition profile vector $[\pi_1(x, t) , \pi_2(x, t), \pi_3(x, t)]$ from three heating and current drive systems. Here we consider input and output variables which are differences between the actual powers or profiles and a reference set of equilibrium parameters and profiles around which the system is linearized. The functions $\pi_1(x, t)$, $\pi_2(x, t)$, $\pi_3(x, t)$, and $y_1(x, t)$, $y_2(x, t)$ are therefore not necessarily positive although we shall still refer to them as the power deposition, safety factor (q) and pressure (or temperature gradient, ρ_T*) profiles. The background process, which governs the plasma response to a change in the input powers and is modeled by the operator $\mathcal{K}$, is assumed to be time-independent. Therefore $\mathcal{K}$ depends on $\tau = t - t'$ in equation (1), and a simple Laplace transformation with respect to time yields the more tractable form :

$$\mathcal{Y}(x,s) = \int_0^1 dx' \quad \mathcal{K}(x,x',s) \bullet \mathcal{P}(x',s) \qquad (2)$$

where, for the sake of simplicity, we use the same symbols for the functions of time and their Laplace transforms. We shall assume that the kernel $\mathcal{K}(x, x', s)$ is square-integrable so that it admits of an infinite singular value expansion in terms of a set of complex orthonormal left and right singular functions, $\mathcal{W}_i(x,s)$ being (2x1) matrices of functions, and $\mathcal{V}_i(x,s)$ being (3x1) matrices of functions, and of the corresponding positive singular values, $\sigma_i(s)$:

$$\mathcal{K}(x,x',s) = \sum_{i=1}^{\infty} \sigma_i(s)\, \mathcal{W}_i(x,s) \bullet \mathcal{V}_i^{+}(x',s) \qquad (3)$$

where + refers to the transconjugate of matrices. Truncating the above expansion to a finite number of terms containing the largest singular values offers the best mean square approximation of the infinite dimension distributed system kernel $\mathcal{K}(x, x', s)$ [22], according to the norm and scalar product which are used to define the orthonormal set of singular functions and which are to be specified later. It is therefore judicious to seek approximate representations of the first left and right singular functions or, here, matrices of functions, and to model the system by the truncated singular value decomposition (TSVD) of the operator $\mathcal{K}(x, x', s)$. Identifying an approximate model for the system thus amounts to identifying its principal components, i.e. the largest significant singular values, $\sigma_i(s)$, together with the corresponding functions $\mathcal{V}_i(x,s)$ and $\mathcal{W}_i(x,s)$. This can only be done from the analysis of a sufficient number of dedicated experiments or simulations, as will be shown later, but we can already anticipate that, with three independent heating and current drive sources, only the first three terms of the expansion can be identified. In what follows we shall therefore assume that the TSVD is to be limited to these first three terms.

For the representation of the left (respectively right) singular functions, a convenient choice is to select a (non necessarily orthonormal) trial function basis which allows a good physical approximation of the various possible output (respectively input) profiles. Assuming that the system responds to three heating and current drive sources (LHCD, NBI and ICRH), one can in principle write the input vector $\mathcal{P}(x, s)$ as :

$$\mathcal{P}(x,s) = \sum_{i=1}^{M} \mathcal{C}_i(x) \bullet \mathbf{P}_i(s) + \text{residual} \qquad (4)$$

where the $\mathcal{C}_i$ matrices are (3x3) trial function matrices built up with the three sets of appropriate basis functions $u_i(x)$, $v_i(x)$ and $w_i(x)$ – which are not necessarily the same sets - and defined by :

$$\mathcal{C}_i(x) = \begin{bmatrix} u_i(x) & 0 & 0 \\ 0 & v_i(x) & 0 \\ 0 & 0 & w_i(x) \end{bmatrix} \qquad (5)$$

and $\mathbf{P}_i(s)$ are (3x1) corresponding input vectors. In order to model the system by its linear response and if the vector $\mathbf{P}_i$ is to contain powers delivered by each actuator, then the space spanned by $u_i(x)$, $v_i(x)$ and $w_i(x)$ should more or less contain the accessible power deposition profiles, possibly divided by the plasma density profile when controlling the current density (current drive efficiencies scale as the inverse of density) or temperature profiles. In equation (4), we assume that a good representation of these profiles can be obtained with a small set of M matrices of basis functions with an input vector corresponding to each of them. In practice, the heating and current drive systems which are generally available on tokamaks have limited active power deposition control and, for the purpose of initial experiments on JET, we shall not consider the possibility that a variety of profiles can in principle be associated to each heating system, For the moment, we shall therefore take M = 1, $u_1(x) = u(x)$, $v_1(x) = v(x)$, $w_1(x) = w(x)$,

$$\mathcal{C}_1(x) = \mathcal{C}(x) = \begin{bmatrix} u(x) & 0 & 0 \\ 0 & v(x) & 0 \\ 0 & 0 & w(x) \end{bmatrix} \qquad (6)$$

and the vector $\mathbf{P}(s) = \mathbf{P}_1(s)$ will contain the three requested input powers. Thus we shall seek representations of $\mathcal{V}_k(x)$, with k=1 to 3, as :

$$\mathcal{V}_k(x,s) = \mathcal{C}(x) \bullet \mathbf{V}_k(s) + \text{residual} \qquad (7)$$

where the $\mathbf{V}_k(s)$ are (3x1) vectors. The matrix of the right singular vectors, $\mathbf{V}_k$, will be called $\mathbf{V}(s)$, i. e. $\mathbf{V}(s) = [\mathbf{V}_1(s)\ \mathbf{V}_2(s)\ \mathbf{V}_3(s)]$. This could be easily generalized to M > 1 if the power deposition profiles were to be varied significantly through external control parameters such as the phasing of the LHCD launcher, for instance, or the ICRH frequency on various antennas, different neutral beam injection angles, different electron cyclotron launch angles, etc...

A possible choice for the output trial function basis is to take a reasonable number (e.g. N = 5 to 10) of cubic splines, $a_i(x)$, to fairly describe the q-profile [note that 1/q could alternatively be chosen, as in [5, 20], for it is an integral of the current density which may be more "linearly" related to the various heating and current drive powers], and possibly the same number of piecewise constant or linear functions, $b_i(x)$, to describe, for instance, the normalised temperature gradient profile (ρ_T^*) so as to allow for a region of large gradient (ITB) where $\rho_T^* > 1.4 \times 10^{-2}$ [19], surrounded by an inner and an outer region of smaller gradients which may not need to be controlled. The choice of these particular dimensionless profiles, q(x) and $\rho_T^*(x)$, is attractive as they take on shapes and absolute values which are characteristic of the discharges as far as transport, turbulence and MHD stability are concerned.

Once the basis functions $a_i(x)$ and $b_i(x)$ have been defined, the output function matrix can be written as :

$$\mathcal{Y}(x,s) = \sum_{j=1}^{N} \mathcal{D}_j(x) \bullet \mathbf{Q}_j(s) + \text{residual} \qquad (8)$$

with

$$\mathcal{D}_j(x) = \begin{bmatrix} a_j(x) & 0 \\ 0 & b_j(x) \end{bmatrix} \qquad (9)$$

and a finite order system which can be identified from experiments and which links the input and output data can be formally written as :

$$\mathbf{Q}(s) = \mathbf{K}(s) \bullet \mathbf{P}(s) \qquad (10)$$

where $\mathbf{Q}(s) = \{\mathbf{Q}_j(s)\}$ is a (2Nx1) column vector obtained by gathering the (2x1) $\mathbf{Q}_j$ components and represents for instance the safety factor and ρ_T^* profiles in the selected basis, **K** is a (2Nx3) matrix and **P** is the input power vector. We shall then also seek representations of $\mathcal{W}_k(x)$, with k=1 to 2N, as :

$$\mathcal{W}_k(x,s) = \sum_{j=1}^{N} \mathcal{D}_j(x) \bullet \mathbf{\Omega}_{kj}(s) + \text{residual} \qquad (11)$$

where the $\mathbf{\Omega}_{kj}(s)$ are (2x1) vectors. For convenience, we combine the (2x1) vectors $\mathbf{\Omega}_{kj}(s)$, for a given k, into a (2Nx1) singular vector, $\mathbf{W}_k$, and the (2Nx2N) matrix made of the left singular vectors will be called **W**(s), i.e. $\mathbf{W}(s) = [\mathbf{W}_1(s)\ \mathbf{W}_2(s)\ \mathbf{W}_3(s) \ldots \mathbf{W}_{2N}(s)]$.

We shall show in subsection 2.2 that the reduction of the infinite system to a finite one, i.e. the identification from experimental data (or from transport code simulations) of $\mathbf{V}_k$, $\mathbf{W}_k$ and σ_k can be done according to a Galerkin scheme in which the residuals are imposed to be spatially orthogonal to each basis trial function. The orthonormality in the space of output functions needs to be defined according to a scalar product and a norm which will ultimately

provide the criterion under which the controller is to minimize the difference vector between the measured profiles and the requested setpoint profiles. For the safety factor profile, q(x), a simple mean square integral,

$$\min \int_0^1 \left[q(x) - q_{setpoint}(x) \right]^2 dx \qquad (12)$$

seems to offer an acceptable criterion. However, because the location of internal transport barriers appears to be closely linked to particular features of the safety factor profiles such as the location of minima or rational values [23, 24], and due to the different time scales under which the pressure and current profiles can evolve, it may be too constraining to impose on the controller a criterion as stringent as (12), both on q and ρ_T*. One could choose for the ρ_T* profile a criterion which leaves more flexibility on the radial location of the ITB, or else, which focusses more on a particular region where the ITB is expected, dismissing the values of ρ_T* elsewhere. For instance, if $\mu(x)$ is a positive weight function which is maximum in the expected region of the ITB, a possible criterion could be :

$$\min \int_0^1 \mu(x) \left[\rho_T^*(x) - \rho_{T,setpoint}^*(x) \right]^2 dx \qquad (13)$$

Since ρ_T* is of order 10^{-2}, the function $\mu(x)$ can also be used to scale expression (13) so that the relative weights of q and ρ_T* in the minimization process are comparable. The corresponding scalar product would then read :

$$\mathcal{Y}_1 \bullet \mathcal{Y}_2 = \int_0^1 dx \; q_1(x) q_2(x) \; + \; \int_0^1 dx \; \mu(x) \rho_{T1}^*(x) \rho_{T2}^*(x) \qquad (14)$$

and the orthonormality of the output singular functions can be written

$$\mathcal{W}_k \bullet \mathcal{W}_{k'} = \delta_{k,k'} \qquad (15)$$

with

$$\mathcal{W}_k \bullet \mathcal{W}_{k'} = \int_0^1 dx \, [\mathcal{W}_k(x)]^+ \bullet \mathcal{J}_1 \bullet [\mathcal{W}_{k'}(x)] + \int_0^1 dx \, \mu(x) \, [\mathcal{W}_k(x)]^+ \bullet \mathcal{J}_2 \bullet [\mathcal{W}_{k'}(x)] \qquad (16)$$

where

$$\mathcal{J}_1 = \begin{bmatrix} 1 & 0 \\ 0 & 0 \end{bmatrix} \qquad \text{and} \qquad \mathcal{J}_2 = \begin{bmatrix} 0 & 0 \\ 0 & 1 \end{bmatrix} \qquad (17)$$

This therefore translates into the matrix equation :

$$\mathbf{W}_k^+ \bullet \mathbf{B} \bullet \mathbf{W}_{k'} = \mathbf{W}_k^+ \bullet \mathbf{\Delta}^+ \bullet \mathbf{\Delta} \bullet \mathbf{W}_{k'} = \hat{\mathbf{W}}_k^+ \bullet \hat{\mathbf{W}}_{k'} = \delta_{k,k'} \qquad (18)$$

where **B** is a (2Nx2N) symmetric positive definite matrix obtained from the scalar products of

the basis functions, made of the (2x2) blocks, $\mathbf{B}_{j,j'}$, defined as

$$\mathbf{B}_{j,j'} = \int_0^1 dx\ \left[\mathcal{D}_j(x)\right]^+ \bullet \mathcal{J}_1 \bullet \left[\mathcal{D}_{j'}(x)\right] + \int_0^1 dx\,\mu(x)\left[\mathcal{D}_j(x)\right]^+ \bullet \mathcal{J}_2 \bullet \left[\mathcal{D}_{j'}(x)\right] \qquad (19)$$

$\mathbf{B} = [\mathbf{\Delta}^+ \bullet \mathbf{\Delta}]$ is its Cholesky decomposition, and $\hat{\mathbf{W}}_k = \mathbf{\Delta} \bullet \mathbf{W}_k$. We thus also have $\hat{\mathbf{W}}^+ \bullet \hat{\mathbf{W}} = \hat{\mathbf{W}} \bullet \hat{\mathbf{W}}^+ = \mathbf{I}_{2N}$ (identity) with $\hat{\mathbf{W}} = \mathbf{\Delta} \bullet \mathbf{W}$.

The orthonormality in the space of the input functions is defined through the usual scalar product and norm :

$$\mathcal{V}_k \ \bullet\ \mathcal{V}_{k'} = \delta_{k,k'} \qquad (20)$$

with

$$\mathcal{V}_k \bullet \mathcal{V}_{k'} = \int_0^1 dx\,[\mathcal{V}_k(x)]^+ \bullet [\mathcal{V}_{k'}(x)] \qquad (21)$$

This translates into the matrix equation :

$$\mathbf{V}_k^+ \bullet \mathbf{A} \bullet \mathbf{V}_{k'} = \mathbf{V}_k^+ \bullet \mathbf{\Gamma}^+ \bullet \mathbf{\Gamma} \bullet \mathbf{V}_{k'} = \hat{\mathbf{V}}_k^+ \bullet \hat{\mathbf{V}}_{k'} = \delta_{k,k'} \qquad (22)$$

where

$$\mathbf{A} = \int_0^1 dx \left[\mathcal{C}\ (x)\right]^+ \bullet \left[\mathcal{C}\ (x)\right] = \mathbf{\Gamma}^+ \bullet \mathbf{\Gamma} \qquad (23)$$

$\hat{\mathbf{V}}_k = \mathbf{\Gamma} \bullet \mathbf{V}_k$ and

$$\mathbf{\Gamma} = \begin{bmatrix} \left[\int_0^1 (u(x))^2\right]^{1/2} & 0 & 0 \\ 0 & \left[\int_0^1 (v(x))^2\right]^{1/2} & 0 \\ 0 & 0 & \left[\int_0^1 (w(x))^2\right]^{1/2} \end{bmatrix} \qquad (24)$$

so that $\hat{\mathbf{V}}^+ \bullet \hat{\mathbf{V}} = \hat{\mathbf{V}} \bullet \hat{\mathbf{V}}^+ = \mathbf{I}_3$ (identity) with $\hat{\mathbf{V}} = \mathbf{\Gamma} \bullet \mathbf{V}$. If u(x), v(x) and w(x) are suitably normalized, $\mathbf{\Gamma}$ can be made unity. With such a normalization $\mathcal{P}(x, t)$ would not correspond to the absorbed power density in the plasma, but this is of minor importance as the multiplication factor can be taken care of by the kernel $\mathcal{K}$.

2.2 Identification of the singular values and singular functions of the distributed system

Let us now return to equation (2) in which we insert the TSVD expansion (3) limited to three terms, as well as the expansions (4), (7), (8) and (11). By left multiplying both sides alternatively by $\mathcal{D}_l^+(x) \bullet \mathcal{J}_l(x)$ and $\mathcal{D}_l^+(x) \bullet \mathcal{J}_2(x)$, performing appropriate integrations over x and summing, one obtains the important relation :

$$\mathbf{B} \bullet \mathbf{Q}(s) = \sum_{k=1}^{3} \sigma_k(s) \left[\mathbf{B} \bullet \mathbf{W}_k(s)\right] \bullet \left[\mathbf{V}_k^+(s) \bullet \mathbf{\Gamma}^+\right] \bullet \left[\mathbf{\Gamma} \bullet \mathbf{P}(s)\right] \qquad (25)$$

which, after left multiplying by $[\boldsymbol{\Delta}^{+}]^{-1}$, yields :

$$[\boldsymbol{\Delta} \bullet \mathbf{Q}(s)] = \sum_{k=1}^{3} \sigma_k(s)\, \hat{\mathbf{W}}_k(s) \bullet \hat{\mathbf{V}}_k^{+}(s) \bullet [\boldsymbol{\Gamma} \bullet \mathbf{P}(s)] \qquad (26)$$

From the definition of the matrix $\mathbf{K}(s)$ which links $\mathbf{Q}(s)$ and $\mathbf{P}(s)$ in equation (10), we can also write :

$$[\boldsymbol{\Delta} \bullet \mathbf{Q}(s)] = [\boldsymbol{\Delta} \bullet \mathbf{K}(s) \bullet \mathbf{P}(s)] = \left[\boldsymbol{\Delta} \bullet \mathbf{K}(s) \bullet \boldsymbol{\Gamma}^{-1}\right] \bullet [\boldsymbol{\Gamma} \bullet \mathbf{P}(s)] \qquad (27)$$

which, by comparing (26) and (27), and by virtue of the orthonormality of the vectors $\hat{\mathbf{W}}_k$ and $\hat{\mathbf{V}}_k$ (cf. eq. 18 and 22), and of the unicity of the SVD expansion, implies that σ_k, $\hat{\mathbf{W}}_k$ and $\hat{\mathbf{V}}_k$ can be found by performing the SVD decomposition of the (2Nx3) matrix $\hat{\mathbf{K}}(s)$ defined by :

$$\hat{\mathbf{K}}(s) = \boldsymbol{\Delta} \bullet \mathbf{K}(s) \bullet \boldsymbol{\Gamma}^{-1} \qquad (28)$$

Once a satisfying model has been experimentally identified for $\mathbf{K}(s)$ by relating the input-output data corresponding to a given set of experiments, $\hat{\mathbf{K}}(s)$ can be easily computed and its SVD can be performed in a straightforward way, yielding :

$$\hat{\mathbf{K}}(s) = \hat{\mathbf{W}}(s) \bullet \boldsymbol{\Sigma}(s) \bullet \hat{\mathbf{V}}^{+}(s) \qquad (29)$$

and the top three rows of $\boldsymbol{\Sigma}(s)$ form a (3x3) diagonal matrix $\tilde{\boldsymbol{\Sigma}}(s)$ and contain the three singular values, $\tilde{\sigma}_1$, $\tilde{\sigma}_2$ and $\tilde{\sigma}_3$, of $\hat{\mathbf{K}}(s)$, which approximate the three largest singular values, σ_1, σ_2 and σ_3, of the infinite dimension operator $\mathcal{K}(x, x', s)$, the other rows being zeros :

$$\tilde{\boldsymbol{\Sigma}}(s) = \begin{bmatrix} \tilde{\sigma}_1(s) & 0 & 0 \\ 0 & \tilde{\sigma}_2(s) & 0 \\ 0 & 0 & \tilde{\sigma}_3(s) \end{bmatrix} \qquad (30)$$

The vectors $\mathbf{V}_k = \boldsymbol{\Gamma}^{-1} \bullet \hat{\mathbf{V}}_k$ and $\mathbf{W}_k = \boldsymbol{\Delta}^{-1} \bullet \hat{\mathbf{W}}_k$, k=1 to 3, then provide the best approximation of the singular functions $\mathcal{V}_i(x,s)$ and $\mathcal{W}_i(x,s)$, on the trial functions basis (cf. eq. 7 and 11), and this completes the identification of the model.

2.3 Pseudo-modal controller design

The TSVD described above has the advantage of providing a reduced order system which best approximates the original system in the mean square sense and retains its distributed nature. Using equations (10), (18), (23), (28) and (29), a truncated diagonal system can then be obtained yielding decoupled open loop relations between modal inputs,

$$\boldsymbol{\alpha}(s) = \mathbf{V}^{+}(s) \bullet \mathbf{A} \bullet \mathbf{P}(s) \qquad (31)$$

and modal outputs

$$\boldsymbol{\beta}(s) = \mathbf{W}^{+}(s) \bullet \mathbf{B} \bullet \mathbf{Q}(s) \qquad (32)$$

namely :

$$\boldsymbol{\beta}(s) = \boldsymbol{\Sigma}(s) \bullet \boldsymbol{\alpha}(s) \qquad (33)$$

Pseudo-modal control techniques can therefore be used by inverting the steady state gain matrix $\tilde{\boldsymbol{\Sigma}}(0)$ and defining $\boldsymbol{\alpha}'(s)$ as $\mathbf{V}(0)^{+} \bullet \mathbf{A} \bullet \mathbf{P(s)}$ and $\boldsymbol{\beta}'(s)$ as $\mathbf{W}(0)^{+} \bullet \mathbf{B} \bullet \mathbf{Q(s)}$ to insure steady state decoupling of the feedback loops. Taking a simple proportional-plus-integral (PI) feedback to eliminate steady state offsets, we thus choose the controller transfer function matrix $\mathbf{G}(s)$ as follows :

$$\boldsymbol{\alpha}'(s) = g_c [1 + 1/(\tau_i.s)] \bullet \boldsymbol{\Sigma}_0^{(-1)} \bullet [\boldsymbol{\beta}'_{setpoint} - \boldsymbol{\beta}'(s)] = G(s) \bullet \boldsymbol{\Sigma}_0^{(-1)} \bullet [\boldsymbol{\beta}'_{setpoint} - \boldsymbol{\beta}'(s)] \qquad (34)$$

where $\boldsymbol{\Sigma}_0^{(-1)}$ is a (3x2N) matrix which left block is $\left[\tilde{\boldsymbol{\Sigma}}(0)\right]^{-1}$, the other columns being filled with zeros, and where g_c is the proportional gain and (g_c/τ_i) is the integral gain. An additional derivative feedback term (PID control) could also be included if it proved necessary to reduce oscillations or for closed loop stability reasons. Thus, setting $\mathbf{V}_0 = \mathbf{V}(0)$, $\mathbf{W}_0 = \mathbf{W}(0)$ and $\boldsymbol{\Sigma}_0 = \boldsymbol{\Sigma}(0)$, we have :

$$\mathbf{P}(s) = g_c [1 + 1/(\tau_i.s)] \bullet \mathbf{V}_0 \bullet \boldsymbol{\Sigma}_0^{(-1)} \bullet \mathbf{W}_0^{+} \bullet \mathbf{B} \bullet [\mathbf{Q}_{setpoint} - \mathbf{Q}(s)] \qquad (35)$$

The resulting feedback control diagram is shown on figure 1.

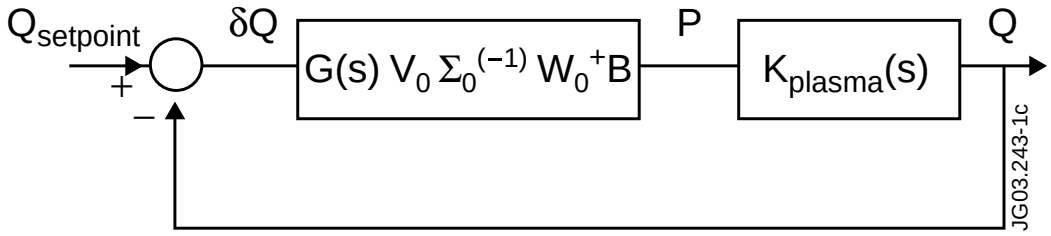

Fig.1. Pseudo-modal feedback loop derived from the TSVD of the kernel $\mathcal{K}(x, x', s)$.

When g_c and τ_i are chosen such as to insure closed loop stability, the controller defined above minimizes the difference between the steady state profiles and the requested ones in the integral least square sense defined in eq.(14), i.e. it realizes :

$$\min\{(\mathbf{Q}^{+}(s=0) - \mathbf{Q}^{+}_{setpoint}) \bullet \boldsymbol{\Delta}^{+} \bullet \boldsymbol{\Delta} \bullet (\mathbf{Q}(s=0) - \mathbf{Q}_{setpoint})\} \qquad (36)$$

or, equivalently when $\mathcal{Y}(s=0)$ and $\mathcal{Y}_{setpoint}$ belong to the space spanned by the chosen set of basis functions,

$$\min \{[\boldsymbol{\gamma}(s=0) - \boldsymbol{\gamma}_{setpoint}] \bullet [\boldsymbol{\gamma}(s=0) - \boldsymbol{\gamma}_{setpoint}]\} \qquad (37)$$

The proof that the closed loop system does converge to this least square difference in steady state, with no offset thanks to the integral feedback term, is given in the appendix.

3. Preliminary experiment on real-time control of the q-profile with LHCD

In order to proceed by small steps in implementing this technique in the elaborate control environment of a device such as JET, it was first chosen to test an SVD pseudo-modal controller based on a real-time reconstruction of the q-profile at 5 plasma radii, yet considering the system as a lumped parameter system relating the normalized input power differences ($\delta\mathbf{P}$) to the five normalized q-differences ($\delta\mathbf{Q}$). The differences were taken between the measured parameters and their values at the end of the reference pulse, and are normalized to these reference values [i.e., we consider the vector elements $\mathbf{P'}_i = \delta\mathbf{P}_i/\mathbf{P}_{i,\,ref} = (\mathbf{P}_i - \mathbf{P}_{i,\,ref})/\mathbf{P}_{i,\,ref}$ and $\mathbf{Q'}_j = \delta\mathbf{Q}_j/\mathbf{Q}_{j,\,ref} = (\mathbf{Q}_j - \mathbf{Q}_{j,\,ref})/\mathbf{Q}_{j,\,ref}$]. The SVD was performed on the dimensionless matrix relating $\mathbf{P'}$ and $\mathbf{Q'}$ ($\mathbf{Q'} = \mathbf{K}_{norm} \bullet \mathbf{P'}$) and the least square minimization will also concern the normalized vector ($\mathbf{Q'} - \mathbf{Q'}_{setpointf}$). This choice is indeed arbitrary. When the distributed character of the system is to be retained, functional representations of the q-profile, e.g. with overlapping splines, will be more appropriate (if the real-time equilibrium reconstruction uses linear combinations of a particular set of trial functions - e.g. polynomials - then one should also take the same set for the controller design). The distributed parameter version of the algorithm will be tested in the near future when attempting to simultaneously control the safety factor (or its inverse) and the ρ_T* profiles. The phasing of the launcher was not varied so that M = 1, and u(x), v(x) and w(x) can be assumed normalised so that $\boldsymbol{\Gamma}$ and $\mathbf{A}$ are also equal to the identity matrix, with a dimension which is the number of actuators used.

The q-profile reconstruction uses the real-time data from the magnetic measurements and from the interfero-polarimetry, and a parameterization of the magnetic flux surface geometry [25, 26]. Later, a more comprehensive real-time Grad-Shafranov solver (EQUINOX) will provide a complete MHD equilibrium [27], but this was not essential for the purpose of the present experiments since we shall assess the performance of the controller by comparing the setpoint profiles with those deduced from the same algorithm as used in the controller. The first, simplest - and in some sense trivial - application of the lumped parameter SVD control scheme was to reach a predefined q-profile with only one actuator, namely LHCD. Since, in this case, the accessible targets are restricted to a one-parameter family of profiles, it is essential that the five q-setpoints are chosen reasonably so that the target q-profile lies close to those in the accessible range. Using only one setpoint around mid-radius could lead to difficulties if the q-profile tends to "rotate" around this radius when varying the power, which is often the case. Using a global parameter such as the internal inductance could put too much weight on the current flowing in the external plasma layers. So, although the control of this scalar parameter could be perfect, i.e. with no steady state offset, some features of the q-profile shape which can be essential for the plasma scenario could be missed (e.g. reverse or weak shear in the plasma core for turbulence stabilization). Applying an SVD technique with five setpoints may not allow to reach any one of the setpoints exactly, but could minimize the error on the profile shape.

The first experiments were performed during an extended LHCD preheat phase [17], a usual prelude to the formation of ITB's in JET. The central electron density was between 1.8 and $1.5x10^{19}m^{-3}$, a relatively low density which allows efficient LHCD. The toroidal field was 3T and in order to be close to a non-inductive steady state regime and thus have a larger flexibility for obtaining non-ohmic reduced-shear q-profiles, the plasma current was chosen to be 1.5MA. The evolution of the main plasma parameters is shown for such a discharge on figure 2a. A linearized lumped-parameter model which links the values of q(r) at five fixed normalised radii (r/a = 0.2, 0.4, 0.5, 0.6, 0.8, with a the minor radius of the plasma and r the radial coordinate) to the input LH power was sought and identified from simple step power changes during dedicated open loop experiments (one without LHCD and the other one with a constant LHCD power of 2.2MW). When only one actuator is used, the steady state gain matrix $\mathbf{K}_{norm}(0)$ is a [5x1] matrix. Thus, in the truncated SVD process we simply write $\mathbf{K}_{norm} = \mathbf{W}\bullet\mathbf{\Sigma}\bullet\mathbf{V}^{+}$, and retain only the first left singular (5x1) vector, $\mathbf{W}_1$, corresponding to the non-zero singular value, $\tilde{\sigma}_1$, and $\mathbf{\Sigma} = \tilde{\sigma}_1$ and $\mathbf{V}$ are therefore scalar matrices. The proportional gain, g_c, was equal to 0.5 and the integral gain, g_c/τ_i, to $1s^{-1}$.

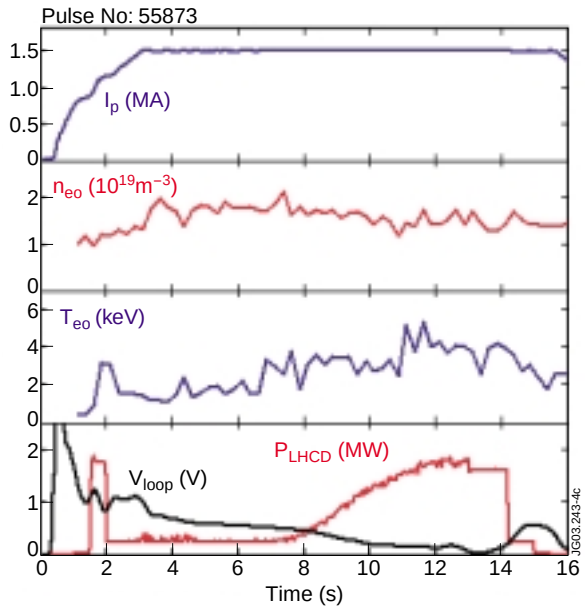

Fig. 2a. Time evolution of the plasma current, I_p, central electron density, n_{e0}, and temperature, T_{e0}, surface loop voltage, V_{loop} and lower hybrid power, P_{LHCD} (pulse #55873, B_T = 3T).

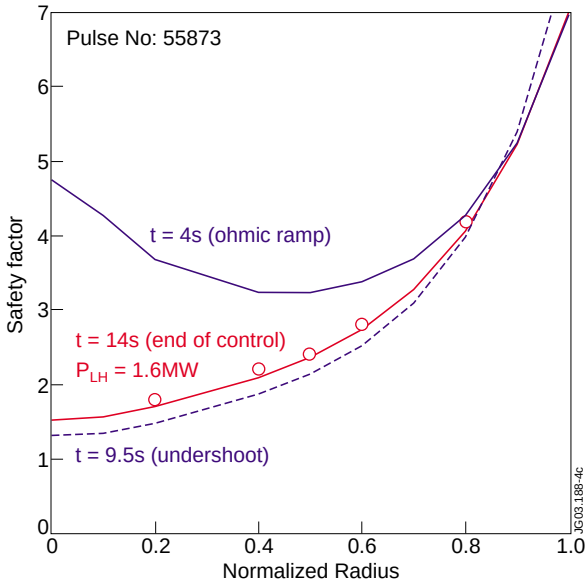

Fig. 2b. Real-time control of the q-profile using LHCD (pulse #55873, B_T = 3T, I_p = 1.5 MA). The profile is shown at three different times including the start (4 s) and the end of the control phase (14 s). Open circles represent the 5 q-setpoints at r/a = [0.2 0.4 0.5 0.6 0.8].

The global result is shown in figure 2b where the requested setpoints are marked as open circles and the measured q-profiles are shown at 3 different times (t = 4 s, 9.5 s and 14 s). The control is only effective after t=7s when the q-profile starts undershooting the setpoints so that the LH power rises. The controller request was negative (so the power was set to zero) during the early relaxation of the strongly reversed profile towards the target. One can see that the target q-profile is fairly well approached at the end of the control phase (t = 14s), the controller minimizing the difference between the 5 target q-values and the corresponding real-

time measurements, in the least square sense. From current diffusion modelling using the CRONOS code [28] the LHCD power deposition profile was found to be off-axis, centred around r/a=0.5 and the fractions of inductive, LH-driven and bootstrap currents were 40%, 53% and 7%, respectively.

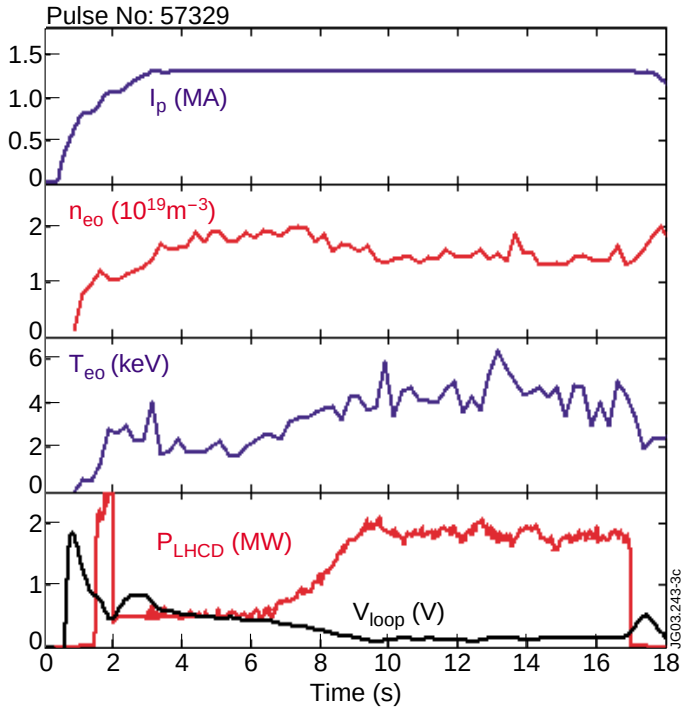

Fig. 3. Time evolution of the plasma current, I_p, central electron density, n_{e0}, and temperature, T_{e0}, surface loop voltage, V_{loop} and lower hybrid power, P_{LHCD} (pulse #57329, B_T = 3T).

Other experiments of the same kind have been recently performed at the same magnetic field (3T) and plasma density ($1.5x10^{19}m^{-3}$) but at lower plasma current (Ip = 1.3 MA, see figure 3) so as to approach a full non-inductive regime during longer pulses and to have more flexibility on the shape of the accessible q-profiles. They have confirmed the effectiveness of the controller in achieving and maintaining in steady state various q-profiles chosen a priori (though reasonably close to the accessible ones), for both monotonic and reversed shear profiles [18]. An illustration of this is shown on figure 4a where the time traces of the real-time measurements of the safety factor at the five selected radii (again, r/a = 0.2, 0.4, 0.5, 0.6, 0.8) are shown together with the setpoint values. The control is effective between t ≈ 8 s and t ≈ 17 s and the five datapoints follow quite nicely the setpoint values. Note that the loop voltage, V_{loop}, is small and constant for about 7 s, as is the internal inductance parameter, l_i, thus confirming the steady state nature of the magnetic equilibrium. CRONOS modelling also indicates that the parallel electric field profile was fairly flat at the end of the control phase so that stationary conditions were reached. A comparison between two pulses with different q-setpoints and one pulse without closed loop control, in similar experimental conditions, is also shown on figure 4b. It shows in particular that the gradual, controlled, application of the LH power does, in real time, prevent the relaxation of the current density towards a more peaked ohmic-like profile.

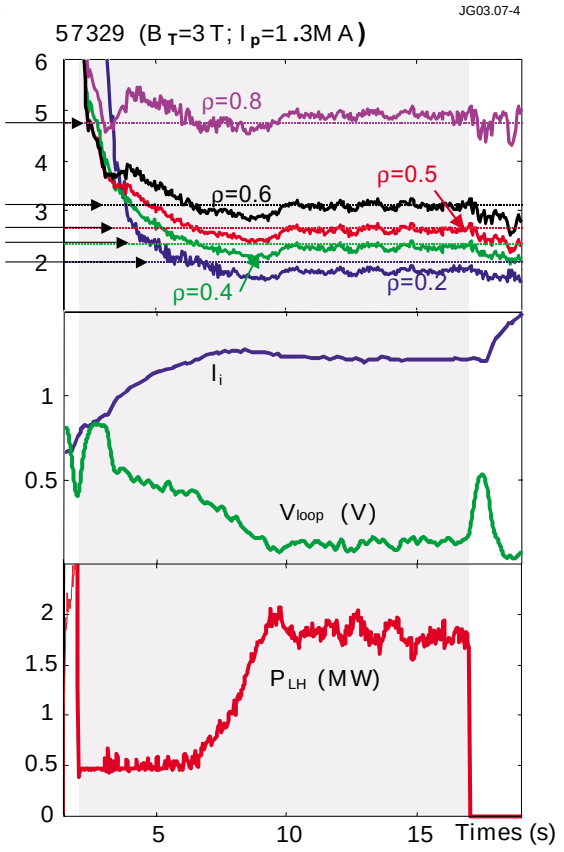

Fig. 4a. Real-time control experiment with LHCD only (pulse #57329, B_T = 3T, I_p = 1.3 MA). Top : Time traces of the safety factor at the five radii selected for the control, r = r/a = [0.2 0.4 0.5 0.6 0.8]. Centre : Time traces of the internal inductance parameter, l_i, and of the surface loop voltage, V_{loop}.(Volts). Bottom : Time trace of the coupled LHCD power (MW).

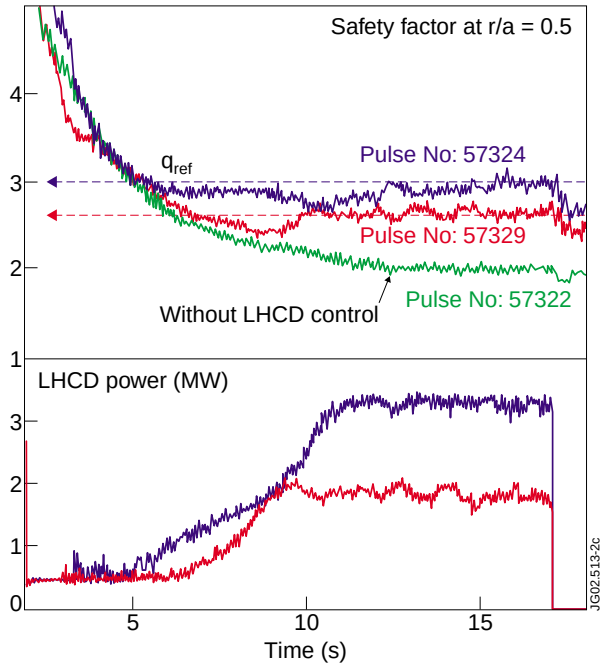

Fig. 4b. Time evolution of the measured and requested q-values at a normalised radius of 0.5 and of the LHCD power waveform for 2 controlled pulses (#57329 and #57324 B_T=3T, Ip=1.3MA). A pulse without feedback control is presented for comparison (#57322). Control starts at 2s and stops at 17s.

4. Real-time control of the q-profile with combined LHCD, NBI and ICRH

The second set of experiments conducted so far and using the proposed model-based TSVD control technique was a first attempt at using the three available heating and current drive systems to control the q-profile during a strong heating phase, in an ITB scenario and with a moderate fraction of the plasma current carried by the bootstrap current. Because of the long current diffusion time scale, it was obvious that the plasma pulse length would have to be as large as possible for the effectiveness of the controller to be assessed, and we therefore selected an advanced plasma scenario which had been developed for long pulses studies. The toroidal magnetic field intensity was 3T and the scenario started with a reversed shear 2.5 MW LHCD preheat phase at a central plasma density around 1.5 x 10^{19} m^{-3} in order to tailor a reversed q-profile in the early stage of the discharge during which the plasma current was ramped up to 1.8 MA. At t ≈ 4 s, 12.5 MW of NBI and 3 MW of ICRH power were applied resulting in a central density of 3 x 10^{19} m^{-3} and in the triggering of an ITB. Then, starting at t = 7 s, the plasma current was ramped down to reach 1.5 MA at t = 11 s, and it remained at this level for another 2 seconds. The very low loop voltage in the final 1.5 MA plateau, indicated that a large fraction of the current was driven by non-inductive sources, including a

significant fraction of bootstrap current. This provided a better target for having access to a wider range of safety factor profiles, monotonic as well as reversed-shear ones.

The determination of the steady state responses to variations of the heating and current drive powers was made from the analysis of four dedicated discharges, including the reference discharge around which the system is to be linearized. In order to have enough flexibility around the reference powers during the real-time control phase, we selected reference powers of 2.5MW, 7MW and 3MW for LHCD, NBI and ICRH, respectively. The scenario described above and which we used for choosing the main discharge parameters for our experiment had shown quite an interesting hysteresis phenomenon when the NBI power was gradually reduced down to 3 MW while the ITB was slowly moving towards the plasma core, but not disappearing [29]. In the reference discharge, we thus chose to reduce abruptly the NBI power from 12.5 to 7 MW at t = 7 s, hoping that the resulting reference plasma would still exhibit an ITB in spite of a quite moderate total heating power. For reasons which may have had to do with the time scale of the power reduction which was different in the two cases and with the ramping down of the plasma current, the hysteresis did not seem to operate and therefore the results which are described below were obtained in conditions with only marginal ITB's ($\rho_T^* \approx 1.5 \times 10^{-2}$) and with a moderate fraction of bootstrap current. Nevertheless they form an interesting basis for further investigations in future high power campaigns.

In the three discharges used for determining the plasma response matrix, $\mathbf{K}_{norm}$, and to keep away from the power limitations of the systems or from the appearance of strong perturbations such as ELM's or MHD instabilities, the LHCD, NBI and ICRH powers were alternately stepped down with respect to the reference ones, always at t = 7 s. The LHCD power was stepped down to 0.5 MW, NBI was stepped down to 11.5 MW (but this corresponds to a step-up with respect to the 7 MW of the reference discharge), and ICRH was stepped down to 0.5 MW. It was found that differences of several megawatts were necessary in order to determine accurately enough the changes in the q-profile, which were averaged between around t ≈ 12.5 s and t ≈ 13 s. This was another reason for stepping down the powers rather than up. The linearity of the q-profile response is of course questionable with differences up to 4.5 MW in the heating power but, as will be shown now, plasma non-linearities were not essential and the controller design, though perhaps not optimal, provided satisfactory results. It will be interesting to check whether this is still the case with stronger ITB's, larger bootstrap current, and when including the ρ_T^* profile in the controlled parameters, in addition to the q-profile.

In analysing the responses given by the real-time data, it was found that the data at r/a=0.8 was corrupted and not quite reliable on one of the previous pulses and we chose r/a = [0.2, 0.4, 0.5, 0.6, 0.7] for the closed-loop control experiments. At these radii, we obtained the following approximate steady state response matrix, in MW^{-1} :

$$\mathbf{K}_{exp}(0) = \begin{bmatrix} 0.0984 & 0.0543 & -0.1530 \\ 0.0849 & 0.0669 & -0.0658 \\ 0.0773 & 0.0707 & -0.0227 \\ 0.0606 & 0.0769 & 0.0104 \\ 0.0474 & 0.0786 & 0.0496 \end{bmatrix}$$

where the actuators are ordered in the sequence [LHCD, NBI, ICRH], and its dimensionless version relating **P**' and **Q**' was :

$$\mathbf{K}_{\text{norm}}(0) = \begin{bmatrix} 0.132 & 0.325 & -0.247 \\ 0.095 & 0.332 & -0.088 \\ 0.076 & 0.310 & -0.027 \\ 0.052 & 0.292 & 0.011 \\ 0.034 & 0.249 & 0.042 \end{bmatrix}$$

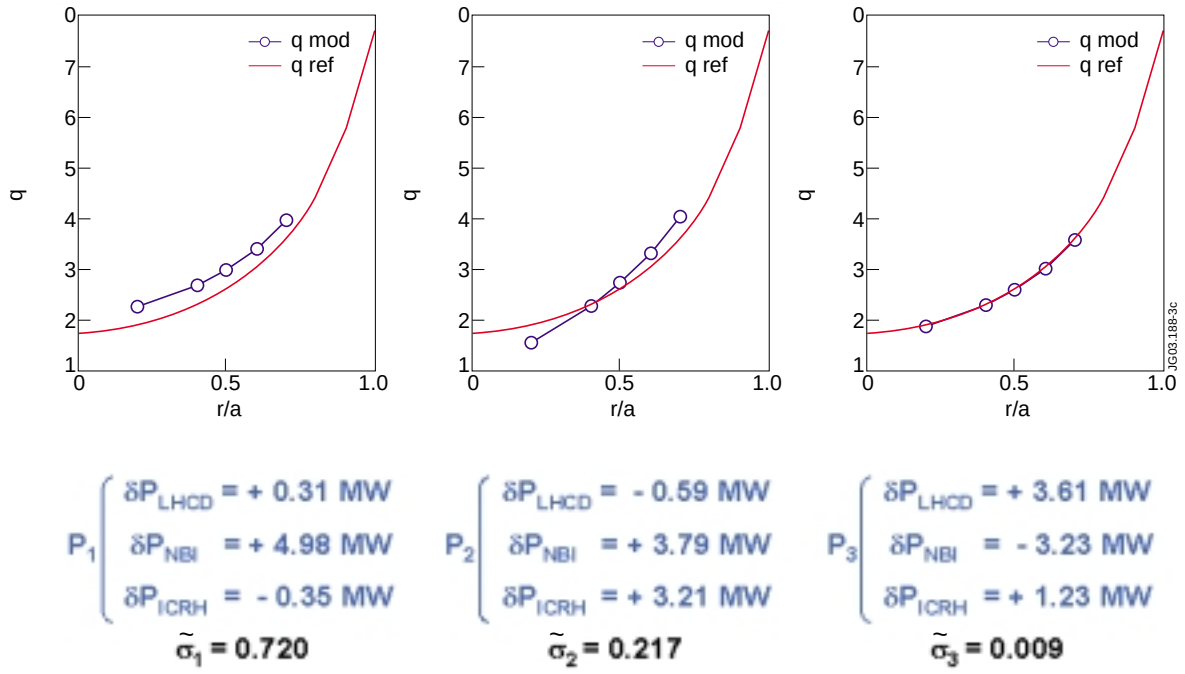

Fig. 5. Respective influence of the 3 identified singular input vectors on the safety factor profile when using simultaneously LHCD, NBI and ICRH as actuators. The full profile which appears in all frames corresponds to the reference equilibrium obtained with P_{LHCD} = 3MW, P_{NBI} = 7MW, P_{ICRH} = 3MW, around which the system is linearized. The open circles on the left, central, and right frames show the q-profiles estimated from the model when adding the power combinations P_1, P_2, and P_3, respectively, to the reference case powers. P_1, P_2, and P_3, are proportionnal to the singular vectors, $\mathbf{V}_1$, $\mathbf{V}_2$, and $\mathbf{V}_3$, but normalized to 5MW. $\tilde{\sigma}_1, \tilde{\sigma}_2$ and $\tilde{\sigma}_3$ are the corresponding singular values.

The singular value decomposition of $\mathbf{K}_{\text{norm}}(0)$ yielded $\tilde{\sigma}_1 = 0.72$, $\tilde{\sigma}_2 = 0.22$, and $\tilde{\sigma}_3 = 0.009$ (which are approximations of σ_1, σ_2 and σ_3, the largest singular values of $\mathcal{K}$), and the following dimensionless singular vectors :

$$\mathbf{V}_0 = \begin{bmatrix} -0.256 & -0.205 & -0.945 \\ -0.936 & 0.297 & 0.190 \\ 0.241 & 0.933 & -0.268 \end{bmatrix}$$

$$\mathbf{W}_0 = \begin{bmatrix} -0.552 & -0.741 & 0.292 & 0.105 & 0.224 \\ -0.494 & -0.014 & -0.328 & -0.563 & -0.575 \\ -0.439 & 0.235 & -0.676 & 0.348 & 0.417 \\ -0.394 & 0.395 & 0.403 & 0.565 & -0.455 \\ -0.322 & 0.490 & 0.433 & -0.481 & 0.488 \end{bmatrix}$$

It was concluded from the ratio between the first and third singular values that the third term in the SVD expansion of the linearized response operator was not significant enough and that this expansion should therefore be truncated to two terms for calculating the controller gain matrix, $\mathbf{V}_0 \bullet \mathbf{\Sigma}_0^{(-1)} \bullet \mathbf{W}_0^{+}$. Using the full operator would have resulted in large matrix elements in the controller gain, due to the largest element in $\mathbf{\Sigma}_0^{(-1)}$. This means that the family of the q-profiles which were effectively accessible with the available heating and current drive systems was indeed a 2-parameter family spanned by $\mathbf{W}_1$ and $\mathbf{W}_2$, and obtained by different linear combinations of the vectors $\mathbf{V}_1$ and $\mathbf{V}_2$, both combining the three LHCD, NBI and ICRH powers. This is illustrated on figure 5 where the respective influence on the q-profile of the three input singular vectors (multiplied by an appropriate numerical factor so that their norms correspond to the same total power of 5MW) is shown, with respect to the reference equilibrium. Clearly the third combination does not play any significant role with reasonable power levels. This situation should change with the addition of the ρ_T* profile in the variables to be controlled, thus enlarging the dimension of the output space in which the system is evolving. We thus expect that all three components of the SVD will provide finite coupled responses when we control the generalized [q(x), ρ_T*(x)] vector.

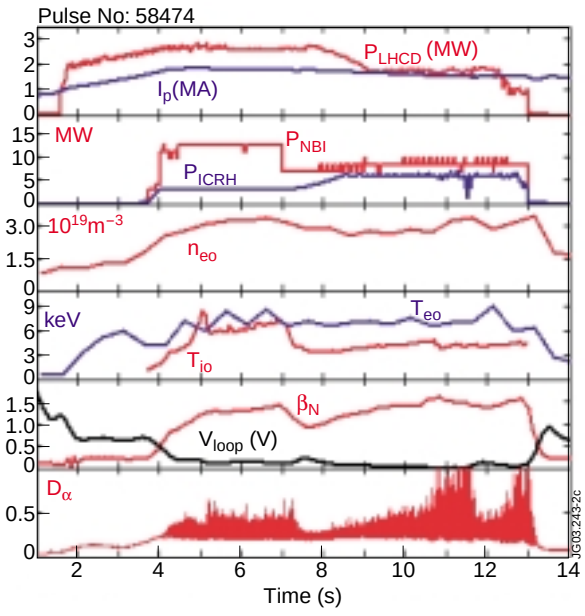

Fig. 6a. Time evolution of the plasma current, I_p, coupled lower hybrid power, P_{LHCD}, ICRH power, P_{ICRH}, NBI power, P_{NBI}, central electron density, n_{e0}, and temperature, T_{e0}, central ion temperature, T_{i0}, surface loop voltage, V_{loop} , normalized β, β_N, and D_α emission (pulse #58474, B_T = 3T).

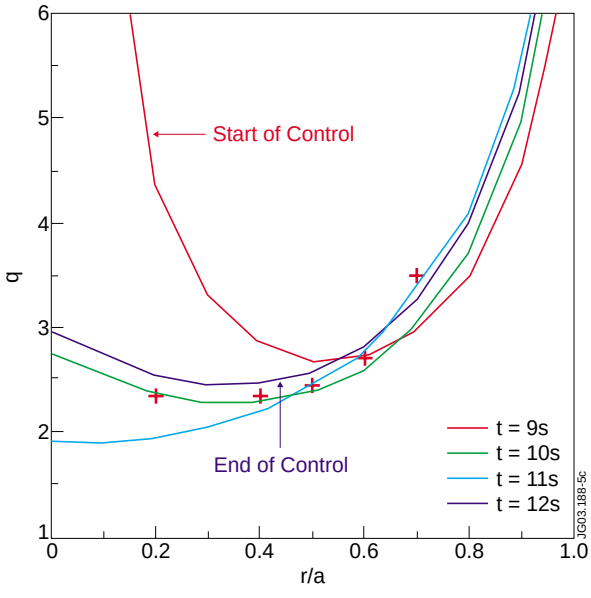

Fig. 6b. Real-time control of the q-profile using LHCD, NBI and ICRH (pulse #58474, B_T = 3T, I_p = 1.8/1.5 MA). The profile is shown at four different times between 7 s and 12 s. Pluses represent the 5 q-setpoints at r/a = [0.2 0.4 0.5 0.6 0.7].

Retaining the first two singular components of the **K**(0) matrix, the following controller gain matrix was obtained (in MW) :

$$\mathbf{G}_{\text{feedback}}(s) = g_C \cdot \left(1 + \frac{1}{\tau_i s}\right) \cdot \begin{vmatrix} 1.20 & 0.21 & -0.06 & -0.20 & -0.25 \\ -1.75 & 3.09 & 3.90 & 3.98 & 3.44 \\ -5.43 & -0.30 & 1.02 & 1.60 & 1.71 \end{vmatrix}$$

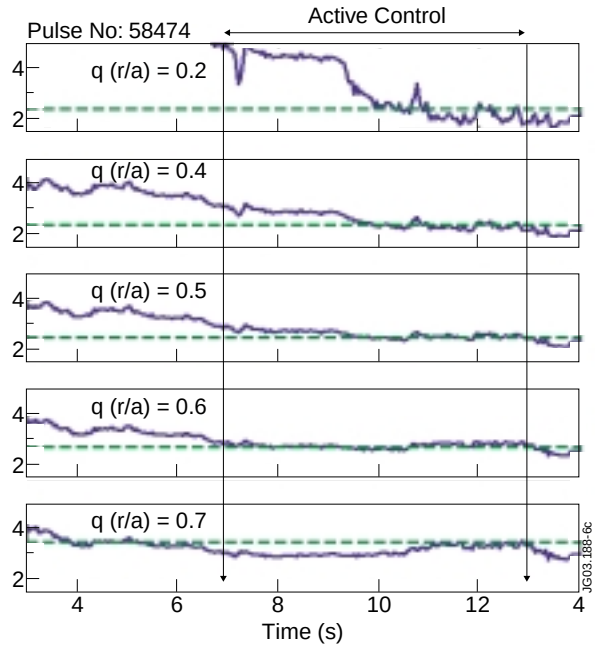

Fig. 7a. Time evolution of the safety factor at the five radii selected for the real-time control experiment of Fig. 6 (pulse #58474, B_T = 3T, I_p = 1.8/1.5 MA). The setpoint values are indicated with dotted lines

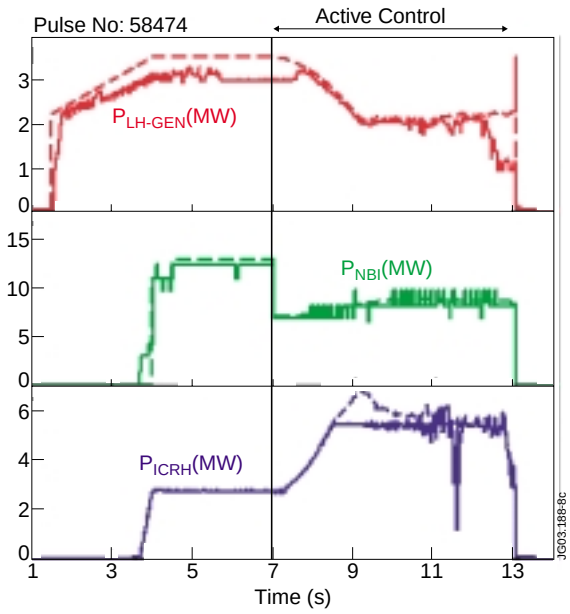

Fig. 7b. Time evolution of the requested (dotted traces) and delivered (full traces) LHCD, NBI and ICRH powers during the real-time control experiment of Fig. 6 (pulse #58474, B_T = 3T, I_p = 1.8/1.5 MA). Note that the LHCD request is applied on the generator power, contrary to NBI and ICRH.

The control was applied between t = 7 s and t = 13 s, with initial powers at the start of the control phase of about 3 MW for LHCD (generator power), 7 MW for NBI (injected power) and 3 MW for ICRH (coupled power). This was assumed to be sufficiently below the limits of the systems to possibly avoid hitting the saturation of an actuator, but in any case, the controller design included a conventional anti-wind-up system to stop integrating the errors when this occurs, or when a negative power is requested. Figures 6 and 7 show the result of a closed-loop experiment in which the controller requests stayed within the bounds allowed by the heating systems. Figure 7b shows a comparison between the requested powers and the achieved ones. During most of the active control phase (i. e. except for short phases when it was limited by protection systems), the LH generator power followed the controller request. NBI was operated in the modulation mode according to which the integrated injected power follows a continuous waveform request on the average. The coupled ICRH power was limited to 6 MW during this pulse, but the controller request was not significantly larger than that. The desired setpoints for q(r/a) at the five selected radii were [2.35 2.34 2.44 2.69 3.5]. The proportional gain, g_c, was equal to 0.1 while the integral gain, g_c/τ_i, was 1 s^{-1}. The q-profile

had a strongly reversed shape at the time when the control started. It then converged slowly towards the desired profile, i.e. towards the closest achievable one, and a minimum of the mean square error was reached at t ≈ 12 s (figure 7a). Despite the fact that the time allowed for the control to be effective was somewhat smaller than the time scale for current diffusion accross the full plasma radius, the selected gains were adequate and the technique was effective. This successful experiment represents a significant result in view of future applications.

5. Conclusion and prospects

A model-based multi-variable scheme is proposed for the real-time control of distributed plasma parameters such as the pressure and safety factor profiles in tokamaks. First experiments using the simplest lumped-parameter versions of the proposed algorithm have been performed in JET. They have shown that the technique can be efficient for obtaining and holding a pre-requested q-profile shape.

A first set of experiments was performed in the low density prelude to the advanced scenarios, in which the current density profile, initially tailored by the application of a given amount of off-axis LHCD current drive during the plasma current ramp up phase, was subsequently controlled in real-time through the proposed SVD feedback scheme, and a steady state magnetic equilibrium was obtained after full relaxation of the ohmic current component throughout the plasma.

Then, more interestingly in view of future high power experiments, a second set of experiments was dedicated to the control of the q-profile during the intense heating phase of advanced scenarios where one expects high plasma performance in JET due to the formation of ITB's, with a good steady state potential due to a large bootstrap current. Although the distributed-parameter version of the algorithm was not yet used, and the various elements of the control scheme (e.g. the identification of the lumped-parameter model and the choice of the PI gains) could not be fully optimized within the allowed experimental time, the safety factor profile was indeed shown to approach a requested profile (as defined by its desired values at five radii) within about 5 s. This is a reasonable time with regard to the full current diffusion time scale in these plasmas. Yet, this was achieved with a marginal ITB and a moderate fraction of bootstrap current, and of course within the limited range of profiles which were accessible with the combination of the ohmic current and of the LH, NBI and ICRH driven currents, at the power levels which were available at the time when the experiments were conducted. The experiments were also partially limited by the available pulse length of the discharges but nevertheless, the achieved plasma state was not far from a steady state equilibrium.

Further experiments in the fully developed ITB regime are definitely required, and will be attempted in the future. Our next goal will be to control simultaneously the current and electron temperature profiles through the generalized [q(x), ρ_T*(x)] vector, using the high resolution real-time electron cyclotron emission (ECE) data, and the real-time magnetic equilibrium reconstruction provided by a new Grad-Shafranov solver (EQUINOX, [27]) integrating the magnetic, interfero-polarimetric and also, later, the motional Stark effect data. The proposed technique, including the identification of a distributed-parameter model with appropriate basis functions, will also be fully exploited and possibly compared with its lumped-parameter version. The ITB temperature gradient control will be attempted either through the maximum value of ρ_T* accross the plasma radius, or through a partial

reconstruction of the ρ_T* profile, retaining only the plasma region where an ITB is expected (and requested) to emerge once a given setpoint q-profile has been chosen. The setpoint ρ_T* profile will be defined using for instance a small set of triangular basis functions (e.g. 3 or 4) which cover this region. In order to retain as much spatial information as possible from the ECE data, the approximate real-time decomposition of the measured ρ_T*profile on this limited basis will be made according to the Galerkin prescription (i.e. by imposing that the residual between the measured and approximate profiles be orthogonal to each basis function).

The various results which are presented in this paper provide an interesting starting basis for a future experimental programme on JET, aiming at the sustainement and real-time control of ITB's in fully non-inductive plasmas and with a significant fraction of bootstrap current. They could represent a significant part of a possible long term experimental programme, including D-T operation on JET and on ITER. The potential extrapolability of the technique to more complex systems with a larger number of controlled parameters (scalars as well as radial profiles) and actuators (possibly with more flexibility in the current deposition profiles, pellet fuelling, ...), is an attractive feature. If the nonlinearities of the system or the difference between various time scales were to be too important, it could also be extended to model-predictive control techniques, at the cost of a larger computational power, and by performing the identification of the full frequency dependence of the linearized response of the system to modulations of the input parameters, rather than simply of its steady state response. It is therefore an interesting method to be considered for an integrated plasma control in view of steady state advanced tokamak operation, including the control of the plasma shape, as in conventional tokamak operation, but also of the primary flux for continuous operation, and of the safety factor, temperature and density profiles, fusion power in a burning plasma, etc... Achieving this goal will represent a major milestone towards the definition and viability of a steady-state tokamak fusion reactor.

Acknowledgements

This work has been performed under the European Fusion Development Agreement (EFDA). The authors are grateful to all the contributors to the EFDA-JET workprogramme, and in particular those involved in the Task Forces S2, H and T, for the preparation and realization of these experiments. The dedicated work of the UKAEA in operating the JET facility is also warmly acknowledged.

Appendix

In this appendix we demonstrate that the pseudo-modal PI controller described in section 2.3 (and sketched in figure 1) minimizes the difference between the steady state output profiles and the requested ones in the least integral mean square sense defined by equations (14) and (37).

Assuming that the identification of the steady state gain matrix $\mathbf{K}(s=0)$ is ideal in that, when multiplied by $\mathbf{P}$, it allows to reproduce exactly the steady state output vector $\mathbf{Q}(s=0)$, then the power vector which minimizes the bracketed expression in (36) is obtained when its variation vanishes for any small variation $\delta\mathbf{P}$ of the vector $\mathbf{P}$, and this occurs if, and only if :

$$\mathbf{K}^{+}(0) \bullet \mathbf{\Delta}^{+} \bullet \mathbf{\Delta} \bullet [\mathbf{K}(0) \bullet \mathbf{P}_{optimal} - \mathbf{Q}_{setpoint}] = \mathbf{0} \qquad \text{(A1)}$$

i.e. :

$$[\boldsymbol{\Delta} \bullet \mathbf{K}(0)]^{+} \bullet [\boldsymbol{\Delta} \bullet \mathbf{K}(0)]\, \mathbf{P}_{\text{optimal}} = [\boldsymbol{\Delta} \bullet \mathbf{K}(0)]^{+} \bullet \boldsymbol{\Delta} \bullet \mathbf{Q}_{\text{setpoint}} \qquad \text{(A2)}$$

or, with (28),

$$\left[\hat{\mathbf{K}}(0) \bullet \boldsymbol{\Gamma}\right]^{+} \bullet \left[\hat{\mathbf{K}}(0) \bullet \boldsymbol{\Gamma}\right] \mathbf{P}_{\text{optimal}} = \left[\hat{\mathbf{K}}(0) \bullet \boldsymbol{\Gamma}\right]^{+} \bullet \boldsymbol{\Delta} \bullet \mathbf{Q}_{\text{setpoint}} \qquad \text{(A3)}$$

This is a (3x3) linear system which can be solved for $\mathbf{P}_{\text{optimal}}$. Multiplying by $[\boldsymbol{\Gamma}^{+}]^{-1}$ and using the SVD (29) and the unitarity of the matrices $\hat{\mathbf{W}}$ and $\hat{\mathbf{V}}$, one comes up with :

$$\mathbf{P}_{\text{optimal}} = \mathbf{V}_0 \bullet [\boldsymbol{\Sigma}_0^{+} \bullet \boldsymbol{\Sigma}_0]^{-1} \bullet \boldsymbol{\Sigma}_0^{+} \bullet \mathbf{W}_0^{+} \bullet \mathbf{B} \bullet \mathbf{Q}_{\text{setpoint}} = [\mathbf{V}_0 \bullet \boldsymbol{\Sigma}_0^{(-1)} \bullet \mathbf{W}_0^{+} \bullet \mathbf{B}] \bullet \mathbf{Q}_{\text{setpoint}} \qquad \text{(A4).}$$

We shall now show that this is indeed what the controller would achieve if the model were ideal, i.e. if the plasma response through $\mathbf{K}_{\text{plasma}}(s)$ could be modeled perfectly with the identified $\mathbf{K}(s)$ and the chosen set of basis functions. With this assumption, the closed loop transfer function of the system is given by :

$$\mathbf{G}_{\text{CL}}(s) = [\mathbf{I} + G(s)\, \mathbf{K}(s) \bullet \mathbf{V}_0 \bullet \boldsymbol{\Sigma}_0^{(-1)} \bullet \mathbf{W}_0^{+} \bullet \mathbf{B}]^{-1} \bullet [G(s)\, \mathbf{K}(s) \bullet \mathbf{V}_0 \bullet \boldsymbol{\Sigma}_0^{(-1)} \bullet \mathbf{W}_0^{+} \bullet \mathbf{B}]$$

$$= [\tau_i\, s\, \mathbf{I} + g_c\,(1+\tau_i\, s)\, \mathbf{K}(s) \bullet \mathbf{V}_0 \bullet \boldsymbol{\Sigma}_0^{(-1)} \bullet \mathbf{W}_0^{+} \bullet \mathbf{B}]^{-1}$$

$$\bullet\, [g_c\,(1+\tau_i\, s)\, \mathbf{K}(s) \bullet \mathbf{V}_0 \bullet \boldsymbol{\Sigma}_0^{(-1)} \bullet \mathbf{W}_0^{+} \bullet \mathbf{B}] \qquad \text{(A5)}$$

and, in the steady state limit ($s \to 0$), the controller achieves :

$$[\mathbf{K}(0) \bullet \mathbf{V}_0 \bullet \boldsymbol{\Sigma}_0^{(-1)} \bullet \mathbf{W}_0^{+} \bullet \mathbf{B}] \bullet \mathbf{Q}(0) = [\mathbf{K}(0) \bullet \mathbf{V}_0 \bullet \boldsymbol{\Sigma}_0^{(-1)} \bullet \mathbf{W}_0^{+} \bullet \mathbf{B}] \bullet \mathbf{Q}_{\text{setpoint}} \qquad \text{(A6).}$$

This does not ensure $\mathbf{Q}(0) = \mathbf{Q}_{\text{setpoint}}$ because $\mathbf{K}$ is a (2Nx3) rectangular matrix and the bracket is therefore singular. However, from eq. (35), the power input vector satisfies :

$$\mathbf{P}(s) = [G(s)\, \mathbf{V}_0 \bullet \boldsymbol{\Sigma}_0^{(-1)} \bullet \mathbf{W}_0^{+} \bullet \mathbf{B}] \bullet [\mathbf{Q}_{\text{setpoint}} - \mathbf{K}(s) \bullet \mathbf{P}(s)] \qquad \text{(A7)}$$

and therefore, with a finite integral gain,

$$[\tau_i\, s\, \mathbf{I} + g_c\,(1+\tau_i\, s)\, \mathbf{V}_0 \bullet \boldsymbol{\Sigma}_0^{(-1)} \bullet \mathbf{W}_0^{+} \bullet \mathbf{B} \bullet \mathbf{K}(s)] \bullet \mathbf{P}(s)$$

$$= g_c\,(1+\tau_i\, s)\, [\mathbf{V}_0 \bullet \boldsymbol{\Sigma}_0^{(-1)} \bullet \mathbf{W}_0^{+} \bullet \mathbf{B}] \bullet \mathbf{Q}_{\text{setpoint}} \qquad \text{(A8)}$$

which in the steady state limit ($s \to 0$) yields :

$$[\boldsymbol{\Sigma}_0^{(-1)} \bullet \mathbf{W}_0^{+} \bullet \mathbf{B} \bullet \mathbf{K}(0)] \bullet \mathbf{P}(0) = [\boldsymbol{\Sigma}_0^{(-1)} \bullet \mathbf{W}_0^{+} \bullet \mathbf{B}] \bullet \mathbf{Q}_{\text{setpoint}} \qquad \text{(A9).}$$

After some algebra, equation (A9) can be rewritten as :

$$[\mathbf{\Sigma}_0^{(-1)} \bullet \mathbf{\Sigma}_0 \bullet \mathbf{V}_0^{+} \bullet \mathbf{A}] \bullet \mathbf{P}(0) = [\mathbf{\Sigma}_0^{(-1)} \bullet \mathbf{W}_0^{+} \bullet \mathbf{B}] \bullet \mathbf{Q}_{\text{setpoint}} \quad \text{(A10).}$$

Now, equation (A10) can be inverted by noting that both $[\mathbf{\Sigma}_0^{(-1)} \bullet \mathbf{\Sigma}_0]$ and $[\mathbf{V}_0^{+} \bullet \mathbf{A} \bullet \mathbf{V}_0]$ are equal to the (3x3) identity matrix, so that finally :

$$\mathbf{P}(0) = [\mathbf{V}_0 \bullet \mathbf{\Sigma}_0^{(-1)} \bullet \mathbf{W}_0^{+} \bullet \mathbf{B}] \bullet \mathbf{Q}_{\text{setpoint}} \qquad \text{(A11)}$$

which, according to eq. (A4), is indeed the optimal steady state power input.

References

[1] Taylor T.S., Plasma. Phys. Control. Fusion **39** (1997) B47.
[2] Gormezano C., Plasma. Phys. Control. Fusion **41** (1999) B367.
[3] Wolf R.C., Plasma. Phys. Control. Fusion **45** (2003) R1.
[4] Jaun A., Fasoli A., Vaclavik J., Villard L., Nucl. Fus. **40** (2000) 1343.
[5] Moreau D., Voitsekhovitch I., Nucl. Fus. **39** (1999) 685.
[6] Wijnands T., Van Houtte D., Martin G., *et al.*, Nucl. Fus. **37** (1997) 777.
[7] Synakowski E.J., Batha S.H., Beer M.A., *et al.*, Phys. Rev. Lett. **78** (1997) 2972.
[8] Ide S., Fujita T., Naito O., Seki M., Plasma. Phys. Control. Fusion **38** (1996) 1645.
[9] Ide S., Fujita T., Suzuki T., *et al.*, Plasma. Phys. Control. Fusion **44** (2002) L63.
[10] Sakamoto Y., Kamada Y., Ide S., *et al.*, Nucl. Fus. **41** (2001) 865.
[11] Wade M., Murakami M., Brennan D.P., *et al.*, "Achieving and Sustaining Steady State Advanced Tokamak Conditions on DIII-D", in Proc. 19th Int. Conf., Lyon 2002 (Vienna, IAEA), paper EX-P3/16.
[12] Rice J. E., Bonoli P. T., Fiore J. L., *et al.*, "Pressure Profile Control of Internal Transport Barrier Plasmas in Alcator C-Mod", Report PSFC/JA-03-3, Plasma Science and Fusion Center, MIT, Cambridge, USA ; to be published in Nucl. Fus. (August 2003).
[13] Crisanti F., Litaudon X., Mailloux J., *et al.*, Phys. Rev. Lett. **88** (2002) 145004.
[14] Litaudon X., Crisanti F., Alper B., *et al.*, Plasma. Phys. Control. Fusion, **44** (2002) 1057.
[15] Litaudon X., Bécoulet A., Crisanti F., *et al.*, Nucl. Fus. **43** (2003) 565.
[16] Mazon D., Litaudon X., Moreau D., *et al.*, Plasma. Phys. Control. Fusion **44** (2002) 1087.
[17] Mazon D., Litaudon X., Moreau D., *et al.*, "Real Time Control of the Current Profile in JET", in Controlled Fusion and Plasma Physics (Proc. 29th Eur. Conf. Montreux, 2002, European Physical Society).
[18] Mazon D., Litaudon X., Moreau D., *et al.*, Plasma. Phys. Control. Fusion **45** (2003) L47.
[19] Tresset G., Litaudon X., Moreau D., Garbet X., Nucl. Fus. **42** (2002) 520.
[20] Moreau D., Kamelander G., Litaudon X., Voitsekhovitch I., J. Plasma Fusion Res. Series, **3** (2000) 502.
[21] Ogunnaike B.A. and Ray W.H., "Process Dynamics, Modelling, and Control", Oxford University Press, Oxford (1994).
[22] Smithies F., "Integral Equations", Cambridge University Press, Cambridge, U. K., 1962.
[23] Garbet X., Baranov Y., Bateman G., *et al.*, "Micro-stability and Transport Modelling of Internal Transport Barriers on JET", in Proc. 19th Int. Conf., Lyon 2002 (Vienna, IAEA), paper TH/C2-1 ; accepted for publication in Nucl. Fus..
[24] Joffrin E., Gorini G., Challis C.D., *et al.*, Plasma. Phys. Control. Fusion **44** (2002) 1739.
[25] Zabeo L., Murari A., Joffrin E., *et al.*, Plasma. Phys. Control. Fusion **44** (2002) 2483.

[26] Riva M., Zabeo L., Joffrin E., *et al.*, "Real Time Safety Factor Profile Determination in JET", Proc. 22th Symp on Fusion Technology (SOFT), Helsinki, Finland (2002).
[27] Bosak K., Blum J., Joffrin E., Sartori F., "Real Time Plasma Magnetic Equilibrium Reconstruction for Tokamaks", to be published in Proc. of the 30th Eur. Conf. on Controlled Fusion and Plasma Physics, St Petersburg, 2003.
[28] Basiuk V., Artaud J.F., Imbeaux F., *et al.*, "Simulations of steady-state scenarios for Tore Supra using the CRONOS code", to be published in Nucl. Fus. (Special Issue, September 2003).
[29] Joffrin E., Crisanti F., Felton R., *et al.*, "Integrated Scenario in JET using Real Time Profile Control", to be published in Proc. of the 30th Eur. Conf. on Controlled Fusion and Plasma Physics, St Petersburg, 2003.